

Redox-Dependent Bone Alkaline Phosphatase Dysfunction Drives Part of the Complex Bone Phenotype in Mice Deficient for *Memo1*

Matthias B Moor,¹ Suresh K Ramakrishnan,¹ Finola Legrand,¹ Silvia Dolder,² Mark Siegrist,² Fanny Durussel,¹ Gabriel Centeno,¹ Dmitri Firsov,¹ Nancy E Hynes,³ Willy Hofstetter,² and Olivier Bonny^{1,4}

¹Department of Pharmacology and Toxicology, University of Lausanne, Lausanne, Switzerland

²Department of Clinical Research, University of Bern, Bern, Switzerland

³Friedrich Miescher Institute for Biomedical Research, Basel, Switzerland

⁴Service of Nephrology, Department of Medicine, Lausanne University Hospital, Lausanne, Switzerland

ABSTRACT

Mediator of ErbB2-driven cell Motility 1 (MEMO1) is an intracellular redox protein that integrates growth factors signaling with the intracellular redox state. We have previously reported that mice lacking *Memo1* displayed higher plasma calcium levels and other alterations of mineral metabolism, but the underlying mechanism was unresolved and the bone phenotype was not described. Here, we show that Cre/lox-mediated MEMO1 deletion in the whole body of C57Bl/6 mice (Memo cKO) leads to severely altered trabecular bone and lower mineralization, with preserved osteoblast and osteoclast number and activity, but altered osteoblast response to epidermal growth factor (EGF) and FGF2. More strikingly, Memo cKO mice display decreased alkaline phosphatase (ALP) activity in serum and in bone, while *ALPL* expression level is unchanged. Bone intracellular redox state is significantly altered in Memo cKO mice and we inferred that ALP dimerization was reduced in Memo cKO mice. Indeed, despite similar ALP oxidation, we found increased ALP sensitivity to detergent in Memo cKO bone leading to lower ALP dimerization capability. Thus, we report a severe bone phenotype and dysfunctional bone ALP with local alteration of the redox state in Memo cKO mice that partially mimics hypophosphatasia, independent of *ALPL* mutations. These findings reveal Memo as a key player in bone homeostasis and underline a role of bone redox state in controlling ALP activity. © 2018 American Society for Bone and Mineral Research

KEY WORDS: MEMO1; ALKALINE PHOSPHATASE; HYPOPHOSPHATASIA; REDOX

Introduction

Hypophosphatasia is a rare autosomal recessive or dominant human disease usually caused by a wide variety of mutations in the *ALPL* gene coding for tissue nonspecific alkaline phosphatase (TNAP). The resulting low alkaline phosphatase (ALP) activity leads to defective bone mineralization with potentially devastating systemic consequences. However, the phenotype is highly variable and milder forms have been described and have broadened the spectrum of the disease.^(1,2)

ALP is a membrane-bound enzyme required for hydrolyzing pyrophosphate and providing cells with an essential source of inorganic phosphate (Pi). Several isoforms of ALP exist in humans, TNAP being predominant and having two main sources: bone and liver. Of note, TNAP is also expressed in the kidney. TNAP monomers need to form intra-chain disulfide bonds in order to assemble into active homodimers,⁽³⁾ further stabilized by Zn⁺⁺ and Mg⁺⁺ ions, and mutations in the

dimerization domain lead to hypophosphatasia.^(4,5) Assembly of the homodimer complex is highly dependent on the redox status surrounding the protein⁽³⁾ and TNAP activity is regulated by the NAD⁺/NADH ratio adenine dinucleotide phosphate (NADH) ratio.⁽⁶⁾

Mediator of ErbB2-driven cell Motility (MEMO) was discovered during a screen for proteins needed for cancer cell migration activated upon ErbB2 receptor phosphorylation.⁽⁷⁾ It is encoded by *MEMO1*, an evolutionary conserved gene that is ubiquitously expressed in mammalian tissues.^(8,9) Intracellular Memo protein is required for cellular responses to heregulin, epidermal and fibroblast growth factors (EGF, FGF), and estrogen.^(7,8,10) Memo protein structure resembles bacterial non-heme iron deoxygenases,⁽¹¹⁾ and Memo was shown to be a copper-dependent redox protein required for reactive oxygen species generation by NADPH oxidase 1.^(12,13) In addition, Memo is involved in essential biological processes, indicated by high conservation of Memo homologs across species from all kingdoms of life and by embryonic lethality of constitutive Memo deletion in mice.^(9,14)

Received in original form September 19, 2017; revised form January 8, 2018; accepted January 14, 2018. Accepted manuscript online January 17, 2018. Address correspondence to: Olivier Bonny, MD, PhD, Department of Pharmacology and Toxicology, University of Lausanne, Rue du Bugnon 27, 1011 Lausanne, Switzerland. E-mail: Olivier.Bonny@unil.ch

Additional Supporting Information may be found in the online version of this article.

JBMR[®] Plus (WOA), Vol. 2, No. 4, July 2018, pp 195–205

DOI: 10.1002/jbm4.10034

© 2018 American Society for Bone and Mineral Research

Thus, Memo is proposed to integrate extracellular signals by modifying the intracellular redox state of the cell.

We have previously reported that postnatally-induced Memo deletion in mice caused a syndrome of premature aging with severe organ atrophies, infertility, insulin hypersensitivity, and disorders of mineral metabolism with elevated 1,25(OH)₂-vitamin D₃ levels and hypercalcemia.⁽⁸⁾

In the current study, we show that Memo is required for normal bone architecture in mice. We further uncovered that loss of the redox protein Memo alters the redox state in the bone, leading to unstable TNAP dimers and functionally inactive ALP, with otherwise unchanged TNAP protein levels. Collectively, our results reveal a new potential cause for hypophosphatasia-related mineral disorders and underscore the role of Memo in controlling bone redox state and bone homeostasis. These results promote *MEMO1* as a candidate gene for hypophosphatasia-like diseases.

Materials and Methods

Animal studies

Animal experiments were performed according to the Swiss guidelines for animal care and were approved by the ad hoc Veterinarian State Committee. Mice were kept under 12:12-hour light/dark conditions and fed a standard laboratory chow (Kliba Nafnag T53242; KLIBA, Kaiseraugst, Switzerland) with free access to food and water. *pCX-CreERTM/Memo^{fl/fl}* mice, as described,⁽⁸⁾ were used as a whole-body inducible Memo cKO model maintained on C57BL/6 background after backcrossing for at least 10 generations. Genotypes were determined by PCR of ear punch biopsy or tail DNA using primers: Memo forward 5'-CCCTCATCTGGCTTGGTA-3', Memo reverse 5'-GCTGCATATGCT-CACAAAGG-3', Cre forward 5'-AGGTCGTGCACTCATGGA-3', Cre reverse 5'-TCACAGTTTATGTTACCC-3'. Recombination was induced by three intraperitoneal injections with 2 mg tamoxifen (Sigma T5648, Buchs, Switzerland) between days 25 to 30 after birth. Memo^{fl/fl} littermates not carrying Cre underwent identical treatment to serve as controls.

For dedicated experiments, mice were kept in metabolic cages (Tecniplast, Buguggiate, Italy) under 12:12-hour light/dark conditions, accustomed for 2 days prior to measurements. Weight was monitored daily.

When needed, mice were anesthetized with ketamine/xylazine and bled by orbital puncture followed by cervical dislocation.

Biochemical analyses

Electrolytes were analyzed by the Lausanne University Hospital: total calcium (NM-BAPTA method), phosphate (phosphomolybdate method), albumin (bromocresol green method), and creatinine (modified Jaffé method). Calcemia was corrected for albumin as described.⁽¹⁵⁾ Sodium and potassium were measured using a flame photometer 943 (Instrumentation Laboratory), osmolality using an osmometer 2020 (Advanced Instrumentation, Inc.), and pH using a pH meter (Metrohm). Inorganic pyrophosphate (iPP) was measured as described.⁽¹⁶⁾ Total pyridoxal-6-phosphate was measured by HPLC at the Swiss Vitamin Institute, Epalinges, Switzerland. ELISA kits were used according to the manufacturers' instructions: FGF23 (Kainos Japan), PTH (Immutopics), osteocalcin (Bioquote by Biomedical Technologies; BT-470), tartrate-resistant acid phosphatase/acid phosphatase 5 tartrate resistant (TRAP/ACP5) (antibodies-online

GmbH), CTX-I (RatLaps), 1,25(OH)₂-vitamin D₃ enzyme immunoassay (EIA) (ImmunoDiagnostic Systems), and 1,25(OH)₂-vitamin D₃ radioimmunoassay (ImmunoDiagnostic Systems). Colorimetric ALP activity (Abcam) and NAD⁺/NADH ratio (Sigma) were measured using commercial kits according to manual instructions. Glomerular filtration rate (GFR) was determined by the method of Qi and colleagues.⁽¹⁷⁾

Cell culture

Mouse long-bone osteocyte-Y4 (MLO-Y4) cells⁽¹⁸⁾ kindly provided by Lynda Bonewald, Indiana University, Indianapolis, IN, USA were maintained on rat-tail type I collagen (Invitrogen by Life Technologies; A10483.01) using alpha-MEM (Gibco by Life Technologies), containing 2.5% calf serum (Sigma), 2.5% fetal calf serum (FCS) (Sigma), and 1% penicillin/streptomycin (Invitrogen by Life Technologies, Carlsbad, CA, USA).

For culture of osteoclast-like cells, femoral marrow cells were harvested from Memo cKO and control mice, treated with 4OH-tamoxifen 1 μM (Sigma) and colony stimulating-factor 1 30 ng/mL (CSF1; PeproTech) for 24 hours, then nonadherent cells were differentiated as described.⁽¹⁹⁾ Differentiation was verified by TRAP activity as described.⁽²⁰⁾ To determine osteoclast resorptive function, ⁴⁵Ca release from calcium phosphate-coated wells was assessed in 96-well plates from the fifth to the sixth day of differentiation and normalized by TRAP activity as described.^(19,21)

Calvaria osteoblasts from Memo cKO and control mice were isolated on postnatal day 1 or 2 by serial digestion using collagenase II (Worthington) in MEM Hank's Medium (Sigma) as described previously.⁽²²⁾ Digestions II to IV were pooled, cultured for 4 days in alpha-MEM + FCS 10% + penicillin/streptomycin 1%, then frozen. Cells were thawed, cultured for 3 days, treated with 4OH-tamoxifen 1 μM for 24 hours, and seeded at 250,000 cells per well in six-well plates. After 7 days, osteogenic differentiation was initiated with alpha-MEM + FCS 10% + penicillin/streptomycin 1% + beta-glycerophosphate 10mM (Sigma) + L-Ascorbic acid 50 μg/mL (Fluka). Medium was freshly prepared three times weekly.

Osteoblasts were fixed with paraformaldehyde (PFA) and stained with Alizarin Red S 2% solution (ScienCell). Alizarin Red S was extracted and quantified as described.⁽²³⁾

Cellular signaling experiments were performed after overnight serum starvation using 100 ng/mL of EGF (Chemie Brunschwig) or FGF2 (SinoBiological).

μCT

Bones were scanned in 70% ethanol on a 1076 machine (Skyscan, Kontich, Belgium) with voxel size 18 μm, filter aluminum (Al) 0.5 mm, exposure 1180 ms, voltage 63 kV, and 166 μA of current. Three-dimensional (3D) reconstructions were visualized by CTVol Version 2.1 (Bruker). BMD was measured in reference to 0.25 and 0.75 g/cm³ calcium phosphate standards with 2 mm diameter (Skyscan). Images were reconstructed using NRecon Version 1.6.9.3 (SkyScan) and analyzed by CTAn Version 1.13.2.1 (SkyScan 2003-11; Bruker 2012-13). Sections 0.5 to 1.5 mm or 2.15 to 2.58 mm from distal growth plate and 0.45 mm of mid-shaft bone between distal growth plate and minor trochanter underwent automated segmentation into cancellous and cortical bone with grayscale thresholds 80/255 and 85/255. L₅ vertebral body trabecular regions were interpolated between three manually selected elliptical planes. Morphometry was obtained using two-dimensional (2D)/3D techniques. Sample sizes required for a power of 0.8 for distal femoral BMD

measurement were estimated as $n = 7$ to 9 per genotype using <http://www.stat.ubc.ca/~rollin/stats/ssize/n2.html> on April 10, 2014.

Bone histomorphometry

Twenty milligrams per kilogram (20 mg/kg) of calcein (Sigma) was intraperitoneally injected in males 2 and 7 days before dissection at age of 62 to 63 days. Femurs were fixed in PFA, washed in 70% ethanol, dehydrated with acetone, and embedded in methyl methacrylate. Longitudinal 4- μ m sections were cut by microtome (RM2255; Leica). Consecutive sections were stained with Von Kossa, 2% Toluidine Blue (pH3.7), mounted with coverslip for dynamic parameter measurement, or stained with TRAP and Toluidine Blue. In addition, PFA-fixed bone was decalcified for 10 days in EDTA 15% - PFA 0.5% and stained for TNAP activity using a commercial kit (Sigma; 85L2-1k5). Morphometric analyses were obtained at magnification $\times 200$ in a 1.8-mm-high \times 0.65-mm-wide region 500 μ m from the distal growth plate and using OsteoMeasure software (Osteometrics Inc., Decatur, GA, USA). Structural parameters BV/TV, Tb.Th, Tb.N, and Tb.Sp were obtained by averaging two measurements from consecutive sections. All parameters are presented according to standardized nomenclature.⁽²⁴⁾

Gene expression

RNA was extracted using TRI reagent (Applied Biosystems by Life Technologies) and reverse transcribed using PrimeScript RT (Takara Bio, Inc.). Standard RT-PCR using GoTaq polymerase (Takara) was performed. qPCR was performed using SYBR Green (Applied Biosystems by Life Technologies) on a 7500 Fast machine (Applied Biosystems) in triplicate. Actin was used as a housekeeping gene for analysis by the delta-delta CT method. Osteoclast gene expression was assessed using TaqMan assays, and CT values were normalized against GUSB gene expression. Melting curves were obtained for every run. Program settings were: 95°C for 20 s, 40 cycles (95°C for 3 s, 60°C for 30 s). Primers were ordered from Microsynth (Balgach, Switzerland); sequences are shown in Supporting Table 2. TaqMan assays-on-demand are indicated in Supporting Table 3. All RNA samples and RT/qPCR products were visualized on agarose gel.

Protein analyses

For standard immunoblotting, proteins of cells and tissues were extracted using NP-40 buffer (50mM HEPES pH 7.4; 150mM NaCl; 25mM NaF; 5mM EGTA; 1mM EDTA; 1% Nonidet P-40; 2M Na ortho-vandate, and 1mM dithiothreitol [DTT] supplied with 10 μ g/L leupeptin [Applichem by Axonlab], 10 μ g/L aprotinin, 1mM phenylmethylsulfonyl fluoride [PMSF]) and lysed using metal beads. Homogenates were spun down for 10 min at 12,000g at 4°C. A total of 10 to 50 μ g of protein was denatured in Laemmli buffer containing a final concentration of 2% beta-mercaptoethanol. For nonreducing conditions beta-mercaptoethanol was omitted. Proteins were separated by 7%, 10%, or 13% SDS-PAGE, transferred on nitrocellulose membranes (PROTRAN; Whatman), and stained with Ponceau S. Membranes were blocked in nonfat dried milk 5%-TBST or bovine serum albumin (Sigma; A9647) 3%-TBST and incubated with primary antibodies detecting Memo,⁽⁸⁾ pERK (Santa Cruz), tERK (Santa Cruz), TNAP/ALP (Abcam), or actin (Sigma) followed by anti-mouse or anti-rabbit horseradish peroxidase-conjugated secondary antibodies (Milian Analytica) and exposure using Fusion Solo (Witec).

For nondenaturing PAGE, femoral marrow was removed by centrifugation, and proteins were extracted from the remaining bone using PBS containing 10 μ g/L leupeptin, 10 μ g/L aprotinin, and 1mM PMSF, followed by addition of a 5 \times sample buffer made from 15.5 mL of 1M Tris-HCl (pH 6.8), 1 mL of bromophenol blue 2.5%, 4.8 mL of distilled H₂O (dH₂O), and 28.7 mL of 87% glycerol with or without 10% of beta-mercaptoethanol (final concentration: 2%). Ten micrograms (10 μ g) of protein was separated on 6% native polyacrylamide gels using a 25mM Tris, 192mM glycine running buffer, followed by immunoblotting as described 1 paragraph above. For protein thiol bioconjugation, PBS-extracted marrow-free femoral protein samples were incubated with AMS (Thermo Fisher Scientific) as described,⁽¹³⁾ prior to PAGE, Ponceau staining, and immunoblotting. All bands were quantified using ImageJ (NIH, Bethesda, MD, USA; <https://imagej.nih.gov/ij/>) and normalized against actin or Ponceau S.

For in-gel ALP staining a method derived from⁽²⁵⁾ was used, with modifications of extraction buffer (ALP assay buffer; Abcam) and staining method. In brief, 10 μ g of protein from marrow-free flushed femur was separated by 10% SDS-PAGE, washed 3 \times 15 min in a wash buffer containing Tris 50mM, NaCl 200mM, CaCl₂ 5mM, ZnSO₄ 5 μ M, Triton 2.5%, and washed 15 min without Triton. Gels were stained for 13 min at room temperature using a commercial ALP staining kit (Sigma).

Statistics

Power analysis was performed before experiments were conducted by using the ClinCal calculator. Statistical differences between two groups were determined using two-tailed unpaired Student's *t* test; $p < 0.05$ was considered significant.

Results

Abnormal bone structure, turnover and mineralization in Memo cKO mice

Memo is expressed in murine bone at all ages (Supporting Fig. 1A) and in several bone-derived cell types (Supporting Fig. 1B, C). To understand the role of Memo in the bone, we used tamoxifen-inducible whole-body Memo cKO mice, as described,⁽⁸⁾ but now backcrossed in the C57Bl/6 background. We verified that the presence of the loxP sites alone or tamoxifen treatment did not affect Memo protein levels in marrow-free femurs of control mice compared to unrelated wild-type mice (Supporting Fig. 1D). We observed efficient loss of Memo protein after tamoxifen treatment in the femur of animals carrying the Cre recombinase (Supporting Fig. 1D).

We further detailed the bone phenotype of Memo cKO mice. Plain X-ray revealed radiolucent distal metaphyseal femur in Memo cKO mice, and reconstruction of micro-computed tomography (μ CT) scans showed a concordant decrease in trabecular bone in the same area, while the volume of cortical bone was increased (Fig. 1A, B). Next, μ CT scans of femurs and vertebrae of mice aged 62 to 63 days were performed. Morphometric analysis of the trabecular bone of distal metaphyseal femur and L₅ vertebrae revealed reduced bone mineral density (BMD), bone volume per total volume (BV/TV), trabecular number (Tb.N), connectivity density (Conn.D), and increased trabecular separation (Tb.S) in Memo cKO (Fig. 1C–F; Supporting Table 1). Trabecular thickness (Tb.Th) was unaffected (Supporting Table 1). Cortical bone was unchanged between genotypes in μ CT analysis at mid-shaft femur (Supporting Table 1), but distal diaphyseal and

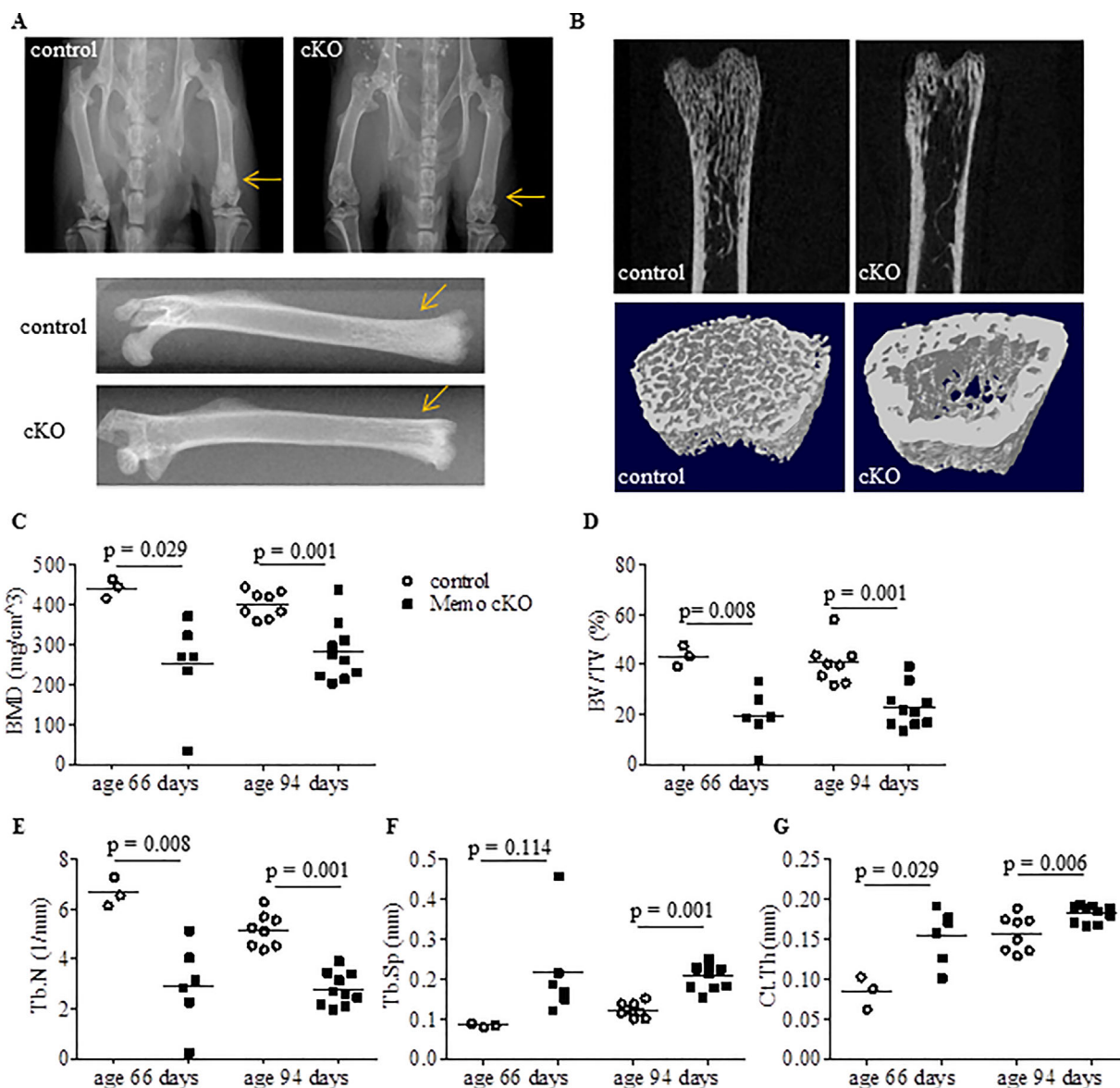


Fig. 1. Abnormal bone structure in Memo cKO mice. (A) X-ray scans of female (top) and male bones (bottom) show alterations in distal metaphyseal femur of Memo cKO (arrows). (B) Mid-section 2D reconstructions (top) and 3D reconstructions (bottom) of μ CT scans show abnormal distal metaphyseal femur in male Memo cKO mice. (A, B) Scans are representative of at least 2 animals per genotype. Morphometric analysis showed lower trabecular BMD (C), BV/TV (D), and Tb.N (E) in Memo cKO males at different ages. Tb.Sp (F) and Ct.Th (G) of distal femoral metaphysis were increased in Memo cKO. (C–G) Animals were dissected 26.4 ± 1.0 days (age 66 days) or 36.7 ± 6.0 days (age 94 days) after tamoxifen treatment. Statistical analysis was done using *t* test. BMD = bone mineral density; BV/TV = bone volume per tissue volume; Tb.N = trabecular number; Tb.Sp = trabecular separation; Ct.Th = cortical thickness.

metaphyseal regions showed excessive cortical thickness in the femur of Memo cKO mice compared to controls (Fig. 1G; Supporting Table 1). Teeth were not affected by loss of Memo in μ CT scans (Supporting Fig. 2).

Histology of nondecalcified femurs from 62-day-old to 63-day-old Memo cKO mice revealed an empty distal femoral metaphysis (Fig. 2A). Histomorphometric analysis showed decreased trabecular BV/TV and Tb.N, and increased Tb.Sp in bones of Memo null animals (Fig. 2B–D). Cortical thickness could not be quantified by histomorphometry in transversal sections of distal femur due to cortical porosity (data not shown).

In dynamic analysis using calcein double labeling, mineral apposition rate (MAR) and bone formation rate per bone volume (BFR/BV) were increased in trabecular bone of Memo cKO mice (Fig. 2E, 2G), whereas mineralizing surface per bone surface (MS/BS) tended to decrease (Fig. 2F). Osteoid thickness (O.Th) was comparable between genotypes (Fig. 2H), but the derived parameters osteoid surface per bone surface (OS/BS) and osteoid volume per bone volume (OV/BV) tended to increase in Memo cKO (Fig. 2I, J).

Collectively, Memo cKO mice display a complex bone phenotype with (i) static bone analyses showing trabecular

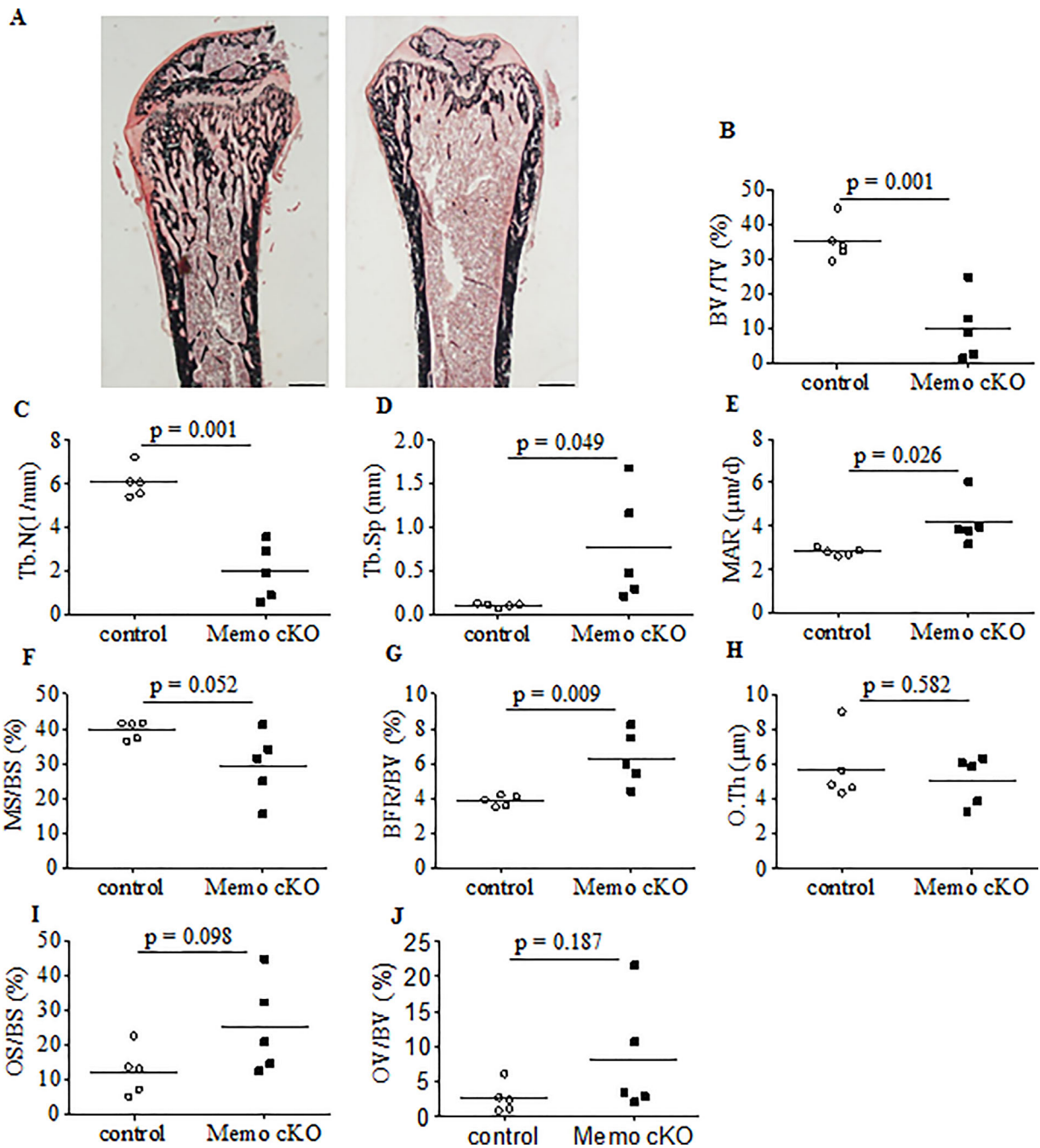


Fig. 2. Altered structure, turnover, and mineralization in femurs of male Memo cKO mice. (A) Von Kossa staining of nondecalcified 4- μ m femoral sections showed scarce trabecular bone in Memo cKO; scale bars = 500 μ m. Histomorphometric analysis revealed lower trabecular BV/TV (B), and Tb.N (C) in Memo cKO. Tb.Sp (D) and MAR (E) were increased in Memo cKO. (F) MS/BS tended to decrease in Memo cKO. (G) BFR/BV was increased in Memo cKO. (H) O.Th was indifferent between genotypes. OS/BS (I) and OV/BV (J) tended to increase in Memo cKO. Mice were dissected 33 to 34 days after tamoxifen treatment at age 62 to 63 days. Statistical analysis was performed by *t* test. BV/TV = bone volume per tissue volume; Tb.N = trabecular number; Tb.Sp = trabecular separation; MAR = mineral apposition rate; MS/BS = mineralizing surface per bone surface; BFR/BV = bone formation rate per bone volume; O.Th = osteoid thickness; OS/BS = osteoid surface per bone surface; OV/BV = osteoid volume per bone volume.

scarcity in femurs and vertebrae, but increased cortical thickness of distal femur; (ii) dynamic assessment showing increased bone formation; and (iii) a clear trend toward impaired mineralization in femurs, because MS/BS tended to decrease and OS/BS and OV/BV to increase.

Normal activity but impaired signaling to growth factors in Memo-deficient bone cells

To gain insight in the mechanisms underlying the structural bone phenotype of Memo cKO mice, we assessed potential

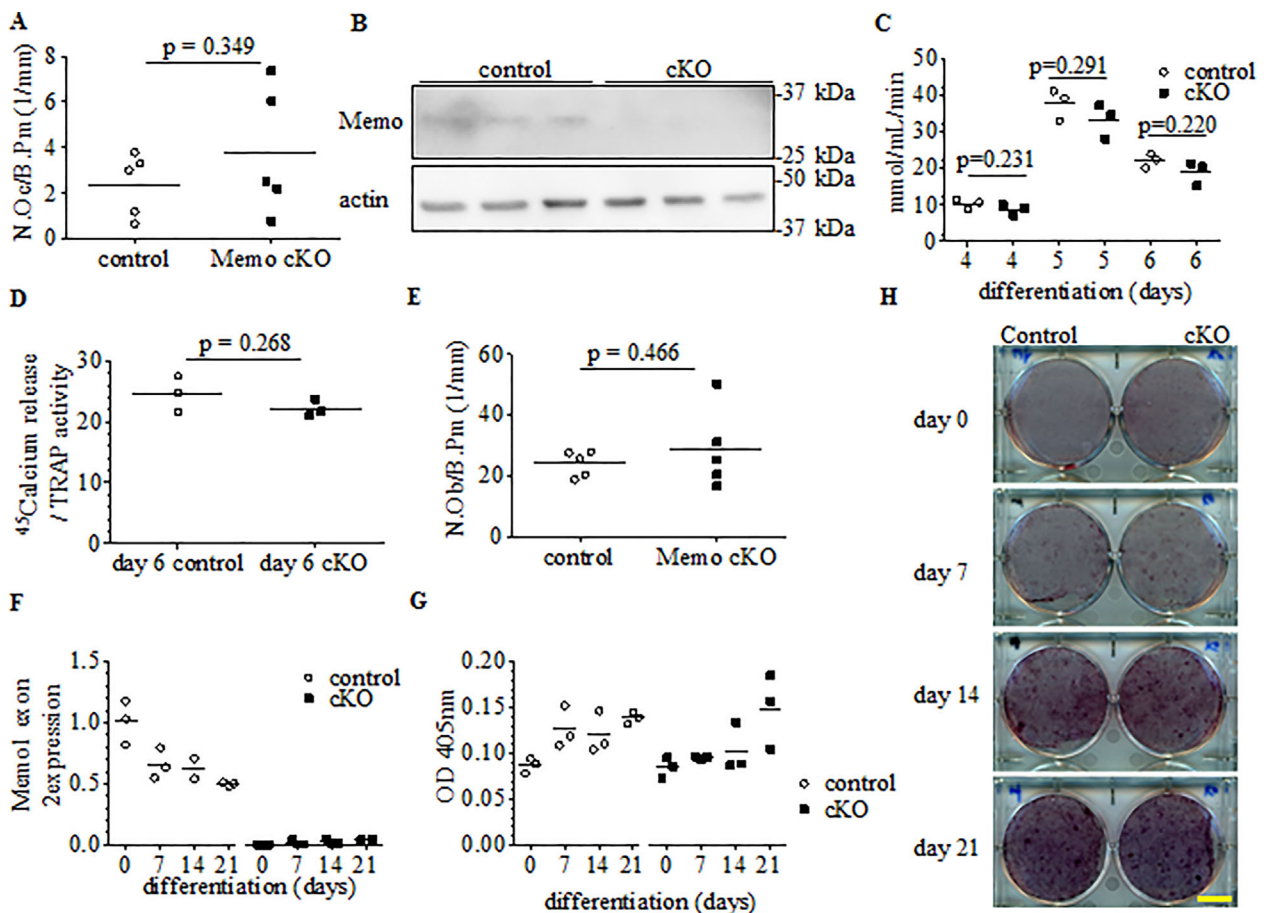


Fig. 3. Unchanged numbers and functional activity of Memo-deficient bone cells. N.Oc/B.Pm (A) and N.Ob/B.Pm (E) were indifferent between genotypes in histomorphometric analysis at age 62 to 63 days, 33 to 34 days after tamoxifen treatment. (B) Western blotting revealed absence of Memo protein in osteoclasts derived from Memo cKO bone marrow progenitors. TRAP activity (C) and resorptive activity of osteoclasts measured by ^{45}Ca resorption over TRAP activity (D) were comparable between genotypes. (F) Memo exon 2 mRNA abundance was analyzed by qPCR in calvaria osteoblasts. (G, H) Mineralization by calvaria osteoblasts was assessed by Alizarin Red S staining and densitometric quantification of eluted Alizarin Red S. Cells were used from 3 independent mice (B–D) or pooled from 16–25 mice (F–H) and analyzed 4 to 6 days (B–D) or 7 to 28 days (F–H) after a 24-hour course of 40H-tamoxifen treatment. (F–H) Pseudoreplicates of pooled cells were thawed and cultured from independent vials. N.Oc/B.Pm = number of osteoclasts per bone perimeter; N.Ob/B.Pm = number of osteoblasts per bone perimeter; TRAP = tartrate-resistant phosphatase.

effects of Memo deletion on bone resorption and mineralization by studying osteoclast and osteoblast number and function *in vivo* and *in vitro*.

The number of osteoclasts per surface was unchanged between genotypes *in vivo* on femoral sections (Fig. 3A). We deleted Memo *ex vivo* in bone marrow-derived cells and differentiated them to osteoclast-like cells. Loss of Memo was verified after 5 days of culture (Fig. 3B; Supporting Fig. 3A). TRAP enzymatic activity peaked 5 days after the start of osteoclast differentiation but was similar between the two genotypes (Fig. 3C). The osteoclasts' resorptive activity, measured by the release of a ^{45}Ca tracer embedded in mineralized culture matrix and normalized by TRAP enzymatic activity, was comparable between control and Memo cKO osteoclast-like cells (Fig. 3D). In addition, expression of osteoclast markers was unchanged in these cells (Supporting Fig. 3).

The number of osteoblasts per surface was unchanged between the two genotypes on bone sections (Fig. 3E). Calvaria osteoblasts showed decreased Memo transcripts upon *ex vivo* Memo deletion (Fig. 3F) but unchanged mineralization activity by Alizarin Red S

staining and elution over 3 weeks of osteogenic differentiation (Fig. 3G, H). However, in line with results from studies on cancer cells,⁽⁷⁾ we detected impaired intracellular growth factor-induced signaling response by ERK phosphorylation in Memo cKO calvaria osteoblasts when these cells were treated with EGF or FGF2 (Fig. 4A; densitometric quantification in Fig. 4B, C). In summary, mineralizing and resorptive function of bone cells were unchanged in *ex vivo* experiments, but Memo was required for normal signaling responses to growth factors in osteoblasts.

Bone-derived hypophosphatasia in Memo cKO mice

To delineate potential alterations in mineral metabolism that could accompany the bone phenotype of Memo cKO mice, we measured serum electrolytes, metabolites, and hormones, as depicted in Table 1. Levels of collagen degradation biomarkers tended to increase, while concentrations of osteoclast TRAP tended to decrease. Serum ALP activity and osteocalcin levels were significantly decreased in sera of Memo cKO mice (Table 1). Memo cKO animals showed higher serum calcium levels,

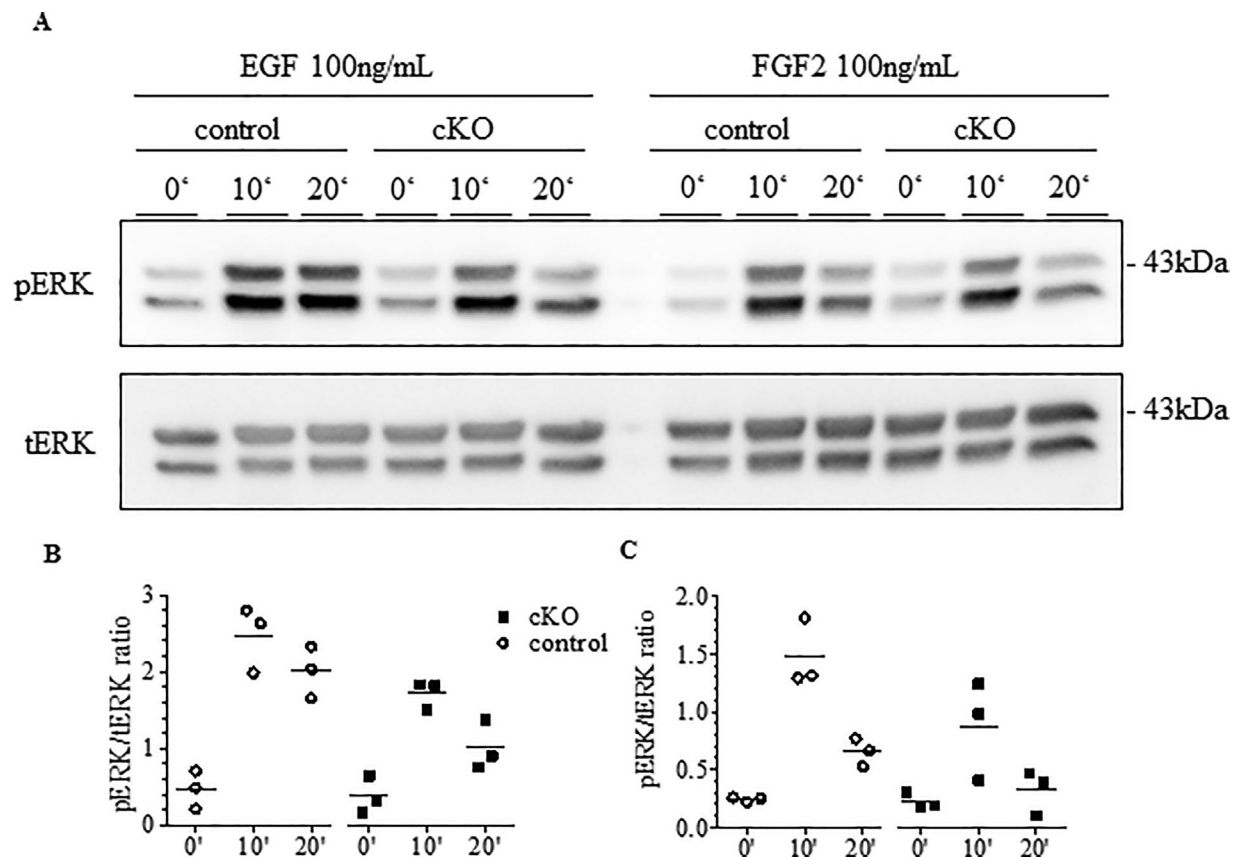


Fig. 4. Memo deletion impairs cellular signaling response to growth factors in osteoblasts. Calvaria osteoblasts were stimulated with EGF or FGF2, and ERK phosphorylation was assessed by Western blot after indicated times. (A) Results representative for experiments of 3 independently thawed cell vials per genotype. Densitometric quantification revealed a blunted phosphorylated over total ERK ratio (pERK, tERK) in Memo null cells after 10 and 20 min of EGF (B) or FGF2 (C) addition. Cells were pooled from 16 to 25 mice and used 13 days after a 24-hour course of 4OH-tamoxifen treatment. Data analysis by ANOVA and Bonferroni's multiple comparisons test. *Significant posttest with $p < 0.05$. ns = nonsignificant posttest; EGF = epidermal growth factor; FGF2 = fibroblast growth factor 2; pERK = phosphorylated ERK; tERK = total ERK.

unchanged phosphatemia, and increased FGF23 levels. Concentrations of bioactive 1,25(OH)₂-vitamin D₃ were unchanged in sera of Memo cKO mice, assessed by two different immunoassays run on two independent set of samples (Table 1).

Next, we collected urine from mice individually held in metabolic cages and we calculated urinary excretion rates of electrolytes normalized by body weight, the latter being smaller in cKO mice (Table 1). Calcium excretion per body weight was 2.5-fold higher in Memo cKO, but excretion rates of all other electrolytes measured, including phosphate, were unchanged. In an analysis of pooled spot urines, Memo cKO mice showed decreased urinary pH and osmolality. In addition, Memo deletion led to increased serum creatinine and a decreased GFR one month after Memo deletion (Table 1).

Because ALP activity was reduced in sera from Memo cKO, and because ALP transforms iPP into inorganic phosphate (Pi), we quantified the excretion rate of iPP in 24-hour urines of Memo cKO animals. We found increased levels of urinary iPP, suggesting that the degree of ALP activity reduction upon Memo deletion was significant enough to detect an increase in the substrate concentration in urine (Table 1). We next determined from which organ a deficiency of functional ALP in the serum was arising. We measured the ALP activity in distal femur, liver, and kidney cortex tissue extracts. Only bone-specific ALP activity was decreased in

Memo cKO mice (Table 1). Similarly, ALP activity staining pattern in bone of Memo cKO was reduced compared to controls (Supporting Fig. 4). However, mRNA expression levels of *ALPL* in tibia and femur were similar between genotypes (Supporting Fig. 5A, B), pointing to a dysfunction of ALP enzymatic activity rather than a lower expression. Noteworthy, expression of selected Wnt pathway genes were normal (Supporting Fig. 5C, D).

Taken together, Memo deletion in mice produced a biochemical profile compatible with disturbed bone mineralization and increased calcium availability from bone, along with lower bone and plasma ALP activity, but otherwise normal tissue *ALPL* expression.

Impaired ALP stability due to altered redox state in femora of *Memo* cKO mice

To test whether the diminished *in vivo* ALP activity could be caused by bone metabolic disturbance upon ablation of the redox protein Memo, we measured the oxidized to reduced NAD ratio (NAD⁺/NADH) in femurs. Indeed, Memo deletion caused an increase in NAD⁺/NADH ratio in marrow-free femurs (Fig. 5A).

Because the enzymatically active form of ALP is a homodimer that relies on oxidation to generate an intrachain disulfide bridge allowing dimerization,⁽³⁾ we assessed

Table 1. Serum, Urine, and Tissue Chemistry of Memo cKO and Controls.

Genotype	Control (mean ± SD)	Memo cKO (mean ± SD)	<i>p</i> (<i>t</i> test)
Serum analyses (<i>n</i> = 6 × 4 pooled per condition)			
ALP activity (U/L)	27.40 ± 3.80	20.01 ± 1.40	0.001
Osteocalcin (ng/mL)	312.32 ± 65.74 ^a	167.87 ± 41.94	0.002
CTX-I (ng/mL)	123.61 ± 17.83 ^a	144.11 ± 17.90	0.091
TRAP (ng/mL)	78.60 ± 10.81	62.53 ± 15.60	0.065
1,25(OH)2-D3 (pM)	105.91 ± 47.65	95.33 ± 32.51	0.663
Intact PTH (pg/mL)	304.96 ± 99.14	307.05 ± 165.96	0.979
Intact FGF23 (pg/mL)	104.61 ± 8.24	424.15 ± 71.44	0.001
Calcium (mM)	2.18 ± 0.03	2.35 ± 0.08	0.001
Corrected calcium (mM)	2.11 ± 0.04	2.30 ± 0.08	< 0.001
Phosphate (mM)	2.11 ± 0.25	1.89 ± 0.14	0.080
Sodium (mM)	152.16 ± 2.01	154.57 ± 2.85	0.121
Albumin (g/L)	34.13 ± 0.95	33.00 ± 0.89	0.060
Creatinine (μM)	7.57 ± 2.48	11.28 ± 2.05	0.018
Pyridoxal-6-phosphate (nM) ^b	897 ± 126	985 ± 265	0.441
24-Hour urine collection (<i>n</i> = 11 controls, 13 cKO)			
Mouse weight (g)	26.69 ± 1.40	24.05 ± 1.12	< 0.001
Urine collected (mL)	1.39 ± 0.40	2.01 ± 1.21	0.120
Inorganic pyrophosphate (mmol/day/g body weight)	0.06 ± 0.11	0.35 ± 0.34	0.014
Calcium (μmol/day/g body weight)	0.17 ± 0.11	0.43 ± 0.40	0.049
Phosphate (μmol/day/g body weight)	3.57 ± 1.82	6.17 ± 5.97	0.180
Sodium (μmol/day/g body weight)	9.46 ± 1.93	9.62 ± 2.31	0.858
Creatinine (μmol/day/g body weight)	0.21 ± 0.05	0.27 ± 0.21	0.367
Pooled spot urines (<i>n</i> = 6 × 4 pooled per condition)			
pH	5.83 ± 0.16	5.54 ± 0.08	0.003
Osmolality (mOsm/kg)	1521 ± 173	1163 ± 245	0.020
Renal function (<i>n</i> = 7 per condition)			
GFR (μL/min)	295.20 ± 32.47	82.96 ± 60.17	< 0.001
Tissue ALP activity (<i>n</i> = 5 per condition)			
Bone ALP activity (U/μg protein)	0.83 ± 0.22	0.36 ± 0.16	0.005
Kidney ALP activity (U/μg protein)	0.01 ± 0.03	0.00 ± 0.00	0.369
Liver ALP activity (U/g protein)	0.17 ± 0.06	0.15 ± 0.15	0.352

Values are mean ± SD. Bold values are significant. Tamoxifen at 56.7 ± 1.5 days and euthanasia after 36.3 ± 4.5 days for serum and spot urines; 27.0 ± 3.9 days for 24-hour urine analysis. GFR was measured at age 98 to 99 days of age. Where indicated, serum or urine was pooled from 4 animals (2 males and 2 females) per analyzed sample. SD = standard deviation; GFR = glomerular filtration rate.

^a*n* = 5 × 4 controls pooled.

^b*n* = 7 per genotype.

ALP protein abundance by native PAGE under reducing and nonreducing conditions and Western blot. In the two conditions, femoral ALP protein quantity or migration pattern between genotypes were similar (Supporting Fig. 6). Next, we generated an oxidation-sensitive adduct by conjugation of 4-acetamido-4'-maleimidylstilbene-2,2'-disulfonic acid (AMS) to reduced thiols. This adduct generated a migration shift of about 20 kDa between reducing and nonreducing conditions on native PAGE in both genotypes, indicating that the bulk of ALP found in the femurs of Memo cKO mice was properly oxidized compared to control mice (Fig. 5B). However, when marrow-free femoral proteins were processed on SDS-PAGE, we detected a 31-fold decreased abundance of ALP dimers and fourfold reduced monomers in Memo cKO compared to controls under nonreducing conditions (Fig. 5C; densitometric quantification in Fig. 5D, E). By in-gel ALP activity assessment, we confirmed that the ALP dimer band separated by SDS-PAGE corresponded to the bioactive form of the enzyme (Fig. 5F; densitometric quantification in Fig. 5G). In summary, we observed altered cellular redox state in femoral bone of Memo cKO. Abundance and oxidation of the ALP enzyme in femoral lysates was comparable between genotypes, but

amounts of enzymatically active dimeric ALP were diminished in bone tissue of Memo cKO after separation by SDS-PAGE.

Discussion

We have identified a severe defect in the trabecular bone of Memo cKO mice using bone histomorphometry and μCT at different sites. Additionally, we observed increased trabecular bone formation and trends to impaired bone mineralization. These observations were accompanied by low bone and serum ALP activity, higher plasma calcium levels with hypercalciuria, and an increased urinary excretion rate of iPP. This bone phenotype, together with the biochemical profile, the presence of a progressive renal failure, and the previously reported muscular hypotonia partially mimics the infantile form of the human disease hypophosphatasia (OMIM #171760).⁽²⁶⁾

As we narrowed down the mechanism of the bone phenotype in Memo cKO mice to a hypophosphatasia-like mineral disorder, evidence indicated that this phenotype was not due to spontaneous mutation of *ALPL*. First, littermate control mice had normal ALP activity. Second, we observed no decrease in

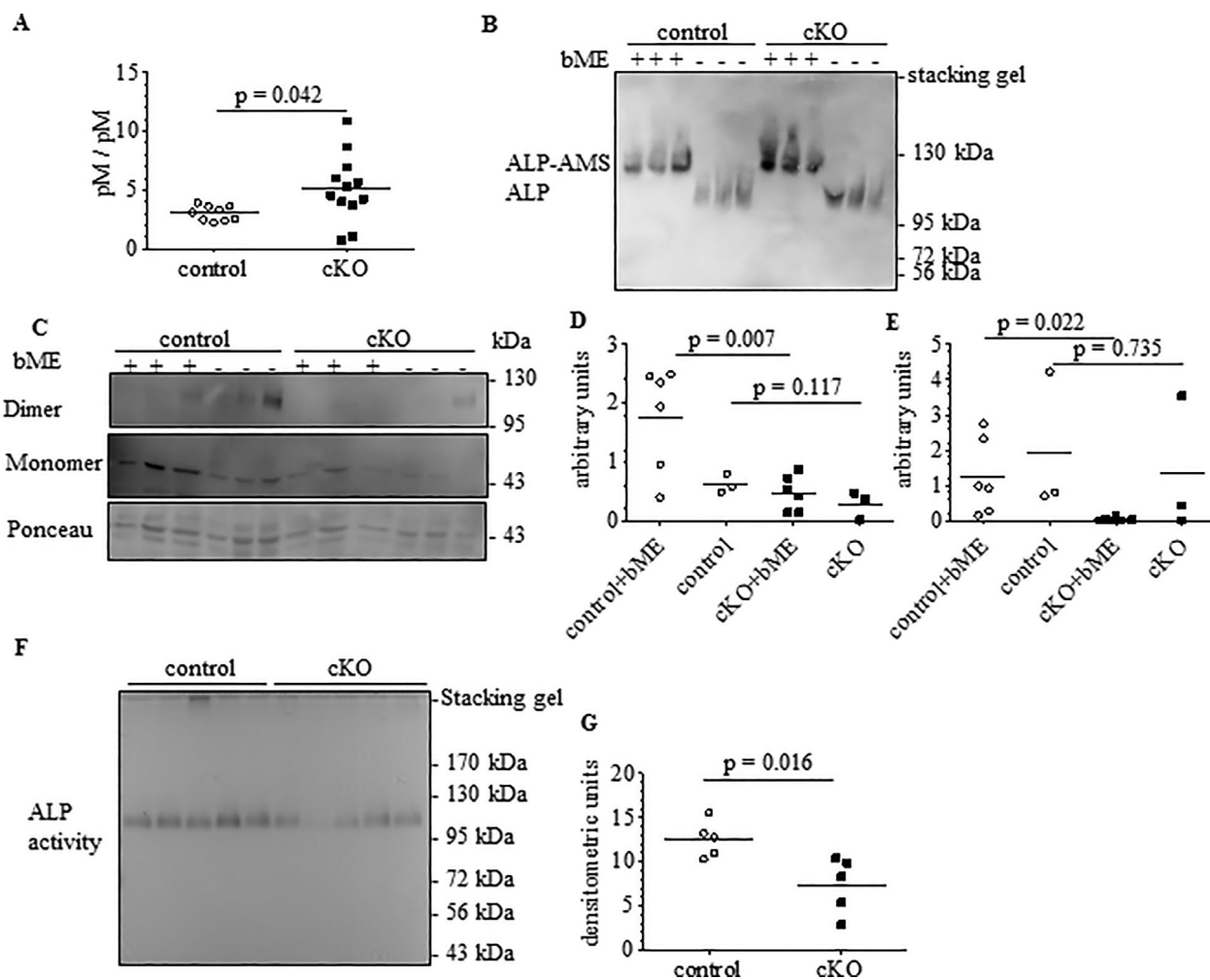


Fig. 5. Memo deletion affects intracellular redox state and SDS stability of femoral ALP. (A) The oxidized to reduced NAD ratio (NAD⁺/NADH) was increased in marrow-free femurs of Memo cKO mice relative to controls. (B) Oxidation-sensitive bioconjugation with AMS revealed indifferently oxidized TNAP in marrow-free femurs of Memo cKO and controls on native gel electrophoresis with or without reduction by 2% β ME. After SDS-PAGE separation, TNAP dimers were 31-fold and monomers fourfold less abundant in bone of Memo cKO compared to controls (C); densitometric quantification in monomers (D) and dimers (E). In-gel activity staining (F) using SDS-PAGE showed that the presumed ALP dimers in C correspond to the bioactive femoral ALP enzyme. In-gel ALP activity was reduced in marrow-free femurs of Memo cKO (F; quantification in G). SDS = sodium dodecyl sulfate; AMS = 4-acetamido-4'-maleimidylstilbene-2,2'-disulfonic acid; TNAP = tissue-nonspecific alkaline phosphatase; β ME = beta-mercaptoethanol.

ALPL gene expression or ALP protein abundance in affected bones. In addition, van Otterloo and colleagues⁽²⁷⁾ recently showed that Memo is required for normal cranial bone development using different perinatal lethal mouse models, indicating that Memo is not only affecting adult ALP activity, but also plays a specific role in early bone development.

When we looked at osteoclasts and osteoblasts of Memo cKO, we did not observe a difference in the number of cells per surface area, suggesting that the bone phenotype is not due to alteration of osteoclast recruitment and/or osteoblast differentiation. In order to further understand the role of Memo in bone, we assessed osteoblast signaling pathways of FGF2 and EGF, two important local growth factors for bone formation.^(28,29) We identified impaired cellular signaling response in Memo cKO mice osteoblasts treated with FGF2 and EGF. Next, we turn to the redox state of the bone, Memo being a redox protein structurally homologous to iron dioxygenases⁽¹¹⁾ and required for NOX1-dependent generation of reactive oxygen species.⁽¹³⁾

We measured NAD⁺/NADH ratio on marrow-free femoral lysates of Memo cKO animals and noticed a shift in the redox state. This reveals an alteration in bone cellular energy homeostasis.

Upon detecting reduced ALP enzymatic activity and a syndrome resembling human hypophosphatasia in our mouse model, we reasoned that a novel form of ALP dysfunction could be present in Memo cKO mice. As cellular redox state was altered in femurs of Memo cKO mice, we hypothesized that the reason for this could be an inadequate dimerization of bone ALP protein due to disturbed oxidation, as has been the case for severe forms of hypophosphatasia with *ALPL* mutations localized in the dimerization domain and preventing the formation of disulfide bonds.⁽³⁾ However, using oxidation-sensitive AMS bioconjugation and non-denaturing gels, we found that femoral ALP protein is similarly oxidized in Memo cKO and controls. But when the samples were run in presence of the detergent SDS, dimeric ALP protein abundance decreased, and enzymatic activity, assessed in gel and corresponding to the molecular mass of dimeric ALP, was

also significantly lower. Thus, femurs of Memo cKO animals showed an altered intracellular redox state in association with increased sensitivity of ALP to SDS. This could be caused by impaired folding of ALP in the endoplasmic reticulum,⁽³⁰⁾ but the present data do not allow determining causality.

Two striking features of Memo cKO mice are the decreased osteocalcin and increased FGF23 concentrations in the serum. Likewise, low serum osteocalcin has been found in hypophosphatasia,⁽³¹⁾ but to our knowledge, FGF23 levels have not been investigated in patients or animal models of hypophosphatasia. Murali and colleagues⁽¹⁶⁾ recently reported that FGF23 decreased *ALPL* gene expression. Additionally, high FGF23 impaired mineralization and caused accumulation of iPP.⁽¹⁶⁾ Further studies should determine if conditions of hypophosphatasia different from those identified in Memo null mice are also associated with excessive FGF23, possibly as a local osteoblast/osteocyte response to disturbed mineralization. Further, levels of 1,25(OH)₂-vitamin D₃ in hypophosphatasia are variable and depend on the degree of hypercalcemia and renal dysfunction.⁽³²⁾ Similarly, in Memo cKO mice on FVB/N × C57BL/6 mixed background, serum 1,25(OH)₂-vitamin D₃ was increased,⁽⁸⁾ whereas the current model on pure C57BL/6 genetic background showed unchanged levels between genotypes.

This study has some limitations. The role of Memo in the bone has been studied in a precisely delimited time window, with induction of the knockout 4 or 8 weeks after birth and all bone studies conducted 4 weeks after induction. At later stages, the bone phenotype might be confounded by other factors related to the model, such as premature aging or the renal insufficiency noted in these mice. The bone phenotype observed did not reveal complete osteomalacia, but only decreased mineral apposition rate, resembling only partially to the bone characteristics of hypophosphatasia. However, *ALPL* null mice⁽³³⁾ develop a radiographic bone phenotype long before (day 9) a demineralizing phenotype is seen by histomorphometry (day 18). Memo cKO mice may develop signs of osteomalacia at later stages, but they die too early to develop it fully. An alternative explanation for the association between hypophosphatasia and bone alterations could be that hypophosphatasia is secondary to the severe bone disease caused by Memo's role in receptor tyrosine kinase signaling. Such a mechanism has been observed in human cases of cleidocranial dysplasia with mutations in the osteoblast transcription factor Runx2.^(34,35)

Another feature of Memo cKO mice unusual for hypophosphatasia-like disorders is the increased cortical bone mass with decreased trabecular bone. This has been described in craniofacial bone, but not for long bone.⁽³⁶⁾ An ambiguous bone defect of opposite trends for trabecular and cortical bone has been described and named "osteopetrorickets" in mice deficient for Sorting Nexin 10, an endosomal trafficking protein.⁽³⁷⁾ In that mouse model, however, the mechanism causing the phenotype was impaired acidification decreasing both osteoclast bone resorption and intestinal calcium absorption.⁽³⁷⁾ Alternatively, disorders of the Wnt pathway have shown diverging phenotypes of cortical versus trabecular bone.⁽³⁸⁾ In summary, a combination of both impaired growth factor signaling affecting the growth plate region and ALP dysfunction may contribute to the opposite cortical and trabecular phenotypes seen in the femur of Memo cKO mice.

To conclude, we showed here that mice devoid of Memo displayed abnormal redox state in bone, dysfunctional ALP activity, and an abnormal bone metabolism and structure (Fig. 6). Overall, these features resemble hypophosphatasia and may explain the higher calcium plasma levels previously

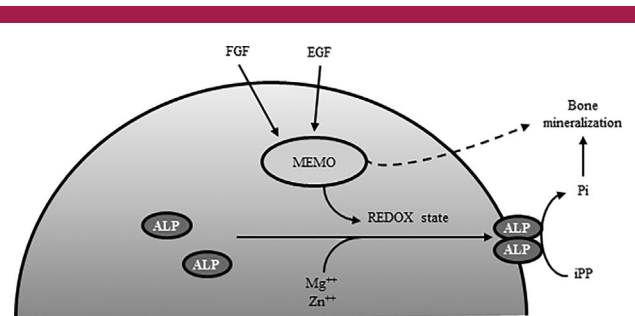


Fig. 6. Working model of Memo's role in bone cells. Memo integrates different extracellular signals and controls ALP dimerization and activity by regulating the local redox state. ALP monomers dimerize by disulfide bridges and are stabilized by divalent ions such as Zn⁺⁺ or Mg⁺⁺. The active ALP dimer catalyzes iPP and frees Pi used for bone mineralization. When Memo is absent, the redox state of the cells is altered and ALP cannot assemble in a dimer or be stabilized by divalent ions leading to decreased activity (hypophosphatasia). Pi cannot be freed from iPP and the iPP/Pi ratio increases. Bone is less mineralized from hypophosphatasia and other bone changes result from Memo-mediated alteration of FGF signaling pathways. ALP = alkaline phosphatase; iPP = inorganic pyrophosphate; Pi = inorganic phosphate.

described in Memo cKO mice.⁽⁸⁾ The Memo null phenotype constitutes a syndrome that significantly differs from phenotypes of other mouse models of low BMD and high serum FGF23 levels, such as *FGF23* overexpressing, *DMP1* KO, or *Hyp* mice, which all showed elevated serum ALP activity.^(39–41) Our results highlight the possibility of alternative causes for hypophosphatasia-like diseases other than mutations in *ALPL*, and related to the Memo-controlled redox state of the bone tissue.

Disclosures

All authors state that they have no conflicts of interest.

Acknowledgments

This work was funded by the NCCR Kidney.CH (to OB and MBM), by the Swiss National Science Foundation to OB (PP00P3-133648), by an unrestricted grant of the Novartis Foundation for Biomedical Research, and by a grant of the patient association "Association pour l'Information et la Recherche sur les Maladies Rénales Génétiques (AIRG-Suisse)." We are thankful to Dorothy Zhang Hu and Roland Baron, Harvard School of Dental Medicine, Boston, MA, USA for bone histomorphometry services. We thank Anna Frei and Florence Morgenthaler for technical support and Pascal Houillier and Barbara Hänzli for helpful discussions and measurement of 1,25-OH₂-vitamin D (PH).

Authors' roles: MBM participated to experimental design; performed experiments; analyzed and interpreted the data; and wrote the paper. SKR performed experiments; and analyzed and interpreted the data. FL performed experiments. SD performed experiments. MS performed experiments. FD performed experiments. GC performed experiments; and analyzed and interpreted the data. DF analyzed and interpreted the data. NEH participated in experimental design; and provided reagents. WH participated in experimental design; and analyzed and interpreted the data. OB participated in experimental design; analyzed and interpreted the data; and wrote the paper.

References

- Rathbun JC. Hypophosphatasia; a new developmental anomaly. *Am J Dis Child.* 1948;75(6):822–31.
- Henthorn PS, Raducha M, Fedde KN, Lafferty MA, Whyte MP. Different missense mutations at the tissue-nonspecific alkaline phosphatase gene locus in autosomal recessively inherited forms of mild and severe hypophosphatasia. *Proc Natl Acad Sci U S A.* 1992;89(20):9924–8.
- Satou Y, Al-Shawafi HA, Sultana S, Makita S, Sohda M, Oda K. Disulfide bonds are critical for tissue-nonspecific alkaline phosphatase function revealed by analysis of mutant proteins bearing a C(201)-Y or C(489)-S substitution associated with severe hypophosphatasia. *Biochim Biophys Acta.* 2012;1822(4):581–8.
- Makita S, Al-Shawafi HA, Sultana S, Sohda M, Nomura S, Oda K. A dimerization defect caused by a glycine substitution at position 420 by serine in tissue-nonspecific alkaline phosphatase associated with perinatal hypophosphatasia. *FEBS J.* 2012;279(23):4327–37.
- Nasu M, Ito M, Ishida Y, et al. Aberrant interchain disulfide bridge of tissue-nonspecific alkaline phosphatase with an Arg433->Cys substitution associated with severe hypophosphatasia. *FEBS J.* 2006;273(24):5612–24.
- Ramasamy I, Butterworth PJ. The inhibition of pig kidney alkaline phosphatase by oxidized or reduced nicotinamide-adenine dinucleotide and related compounds. *Biochem J.* 1973;131(2):359–67.
- Marone R, Hess D, Dankort D, Muller WJ, Hynes NE, Badache A. Memo mediates ErbB2-driven cell motility. *Nat Cell Biol.* 2004;6(6):515–22.
- Haenzi B, Bonny O, Masson R, et al. Loss of Memo, a novel FGFR regulator, results in reduced lifespan. *FASEB J.* 2014;28(1):327–36.
- Schlatter ID, Meira M, Ueberschlag V, Hoepfner D, Movva R, Hynes NE. MHO1, an evolutionarily conserved gene, is synthetic lethal with PLC1; Mho1p has a role in invasive growth. *PLoS One.* 2012;7(3):e32501.
- Frei A, MacDonald G, Lund I, Gustafsson JA, Hynes NE, Nalvarte I. Memo interacts with c-Src to control Estrogen Receptor alpha subcellular localization. *Oncotarget.* 2016;7(35):56170–82.
- Qiu C, Lienhard S, Hynes NE, Badache A, Leahy DJ. Memo is homologous to nonheme iron dioxygenases and binds an ErbB2-derived phosphopeptide in its vestigial active site. *J Biol Chem.* 2008;283(5):2734–40.
- Ewald CY, Hourihan JM, Bland MS, et al. NADPH oxidase-mediated redox signaling promotes oxidative stress resistance and longevity through memo-1 in *C. elegans*. *Elife.* 2017;6. DOI:10.7554/eLife.19493
- MacDonald G, Nalvarte I, Smirnova T, et al. Memo is a copper-dependent redox protein with an essential role in migration and metastasis. *Sci Signal.* 2014;7(329):ra56.
- Kondo S, Bottos A, Allegood JC, et al. Memo has a novel role in S1P signaling and crucial for vascular development. *PLoS One.* 2014;9(4):e94114.
- Hough TA, Bogani D, Cheeseman MT, et al. Activating calcium-sensing receptor mutation in the mouse is associated with cataracts and ectopic calcification. *Proc Natl Acad Sci U S A.* 2004;101(37):13566–71.
- Murali SK, Roschger P, Zeitz U, Klaushofer K, Andrukhova O, Erben RG. FGF23 regulates bone mineralization in a 1,25(OH)₂D₃ and Klotho-independent manner. *J Bone Miner Res.* 2016;31(1):129–42.
- Qi Z, Whitt I, Mehta A, et al. Serial determination of glomerular filtration rate in conscious mice using FITC-inulin clearance. *Am J Physiol Renal Physiol.* 2004;286(3):F590–6.
- Kato Y, Windle JJ, Koop BA, Mundy GR, Bonewald LF. Establishment of an osteocyte-like cell line, MLO-Y4. *J Bone Miner Res.* 1997;12(12):2014–23.
- Albano G, Moor M, Dolder S, et al. Sodium-dependent phosphate transporters in osteoclast differentiation and function. *PLoS One.* 2015;10(4):e0125104.
- Dolder S, Hofstetter W, Wetterwald A, Muhlbauer RC, Felix R. Effect of monoterpenes on the formation and activation of osteoclasts in vitro. *J Bone Miner Res.* 2006;21(4):647–55.
- Xie W, Lorenz S, Dolder S, Hofstetter W. Extracellular iron is a modulator of the differentiation of osteoclast lineage cells. *Calcif Tissue Int.* 2016;98(3):275–83.
- Xie W, Dolder S, Siegrist M, Wetterwald A, Hofstetter W. Glutamate receptor agonists and glutamate transporter antagonists regulate differentiation of osteoblast lineage cells. *Calcif Tissue Int.* 2016;99(2):142–54.
- Tavakol S, Ragerdi Kashani I, Azami M, et al. In vitro and in vivo investigations on bone regeneration potential of laminated hydroxyapatite/gelatin nanocomposite scaffold along with DBM. *J Nanopart Res.* 2012;14(12):1–14.
- Dempster DW, Compston JE, Drezner MK, et al. Standardized nomenclature, symbols, and units for bone histomorphometry: a 2012 update of the report of the ASBMR Histomorphometry Nomenclature Committee. *J Bone Miner Res.* 2013;28(1):2–17.
- Martin S, Lin H, Ejimadu C, Lee T. Tissue-nonspecific alkaline phosphatase as a target of sFRP2 in cardiac fibroblasts. *Am J Physiol Cell Physiol.* 2015;309(3):C139–47.
- Fraser D. Hypophosphatasia. *Am J Med.* 1957;22(5):730–46.
- Van Otterloo E, Feng W, Jones KL, et al. MEMO1 drives cranial endochondral ossification and palatogenesis. *Dev Biol.* 2016;415(2):278–95.
- Kim HJ, Kim JH, Bae SC, Choi JY, Kim HJ, Ryoo HM. The protein kinase C pathway plays a central role in the fibroblast growth factor-stimulated expression and transactivation activity of Runx2. *J Biol Chem.* 2003;278(1):319–26.
- Marie PJ, Hott M, Perheentupa J. Effects of epidermal growth factor on bone formation and resorption in vivo. *Am J Physiol.* 1990;258(2 Pt 1):E275–81.
- Ey PL, Ferber E. Calf thymus alkaline phosphatase. I. Properties of the membrane-bound enzyme. *Biochim Biophys Acta.* 1977;480(2):403–16.
- Nangaku M, Sato N, Sugano K, Takaku F. Hypophosphatasia in an adult: a case report. *Jpn J Med.* 1991;30(1):47–52.
- Fallon MD, Teitelbaum SL, Weinstein RS, Goldfischer S, Brown DM, Whyte MP. Hypophosphatasia: clinicopathologic comparison of the infantile, childhood, and adult forms. *Medicine (Baltimore).* 1984;63(1):12–24.
- Fedde KN, Blair L, Silverstein J, et al. Alkaline phosphatase knock-out mice recapitulate the metabolic and skeletal defects of infantile hypophosphatasia. *J Bone Miner Res.* 1999;14(12):2015–26.
- Morava E, Kartesz J, Weisenbach J, Caliebe A, Mundlos S, Mehес K. Cleidocranial dysplasia with decreased bone density and biochemical findings of hypophosphatasia. *Eur J Pediatr.* 2002;161(11):619–22.
- Unger S, Mornet E, Mundlos S, Blaser S, Cole DE. Severe cleidocranial dysplasia can mimic hypophosphatasia. *Eur J Pediatr.* 2002;161(11):623–6.
- Liu J, Nam HK, Campbell C, Gasque KC, Millan JL, Hatch NE. Tissue-nonspecific alkaline phosphatase deficiency causes abnormal craniofacial bone development in the *Alpl(-/-)* mouse model of infantile hypophosphatasia. *Bone.* 2014;67:81–94.
- Ye L, Morse LR, Zhang L, et al. Osteopetrorickets due to *Snx10* deficiency in mice results from both failed osteoclast activity and loss of gastric acid-dependent calcium absorption. *PLoS Genet.* 2015;11(3):e1005057.
- Simsek Kiper PO, Saito H, Gori F, et al. Cortical-bone fragility—insights from sFRP4 deficiency in Pyle’s disease. *N Engl J Med.* 2016;374(26):2553–62.
- Shimada T, Mizutani S, Muto T, et al. Cloning and characterization of FGF23 as a causative factor of tumor-induced osteomalacia. *Proc Natl Acad Sci U S A.* 2001;98(11):6500–5.
- Feng JQ, Ward LM, Liu S, et al. Loss of DMP1 causes rickets and osteomalacia and identifies a role for osteocytes in mineral metabolism. *Nat Genet.* 2006;38(11):1310–5.
- Rowe PS, Matsumoto N, Jo OD, et al. Correction of the mineralization defect in hyp mice treated with protease inhibitors CA074 and pepstatin. *Bone.* 2006;39(4):773–86.